Online ISSN 1848-3380, Print ISSN 0005-1144
ATKAFF 57(2), 319–328(2016)

Evren Isen, Ahmet Faruk Bakan

Development of 10 kW Three-Phase Grid Connected Inverter

DOI 10.7305/automatika.2016.10.1081
UDK [621.314.572.025.3.026.44:519.673]:621.376

Original scientific paper

In this paper, modeling, simulation and experimental study of a 10 kW three-phase grid connected inverter are presented. The mathematical model of the system is derived, and characteristic curves of the system are obtained in MATLAB with m-file for various switching frequencies, dc-link voltages and filter inductance values. The curves are used for parameter selection of three-phase grid connected inverter design. The parameters of the system are selected from these curves, and the system is simulated in Simulink. Modeling and simulation results are verified with experimental results at 10 kW for steady state response, at 5 kW for dynamic response and at -3.6 kVAr for reactive power. The inverter is controlled with Space Vector Pulse Width Modulation technique in d-q reference frame, and dSPACE DS1103 controller board is used in the experimental study. Grid current total harmonic distortion value and efficiency are measured 3.59% and 97.6%, respectively.

Key words: Grid Connected Inverter, Inverter Modeling, Space Vector Pulse Width Modulation, Total Harmonic Distortion.

Razvoj 10 kW trofaznog izmjenjivača spojenoga na mrežu. U ovom radu prikazano je modeliranje, simuliranje i eksperimentalno istraživanje 10 kW trofaznog izmjenjivača spojenoga na mrežu. Izveden je matematički model te su u MATLAB-u uz korištenje m-skripti dobivene karakteristične krivulje sustava za različite preklopne frekvencije, napone dc-linka i vrijednosti induktiviteta filtra. Krivulje su korištene za odabir parametara dizajna trofaznog izmjenjivača spojenoga na mrežu. Parametri sustava su odabrani iz krivulja, a sustav je simuliran u Simulinku. Rezultati modeliranja i simuliranja eksperimentalno su verificirani na 10 kW odziva u stacionarnom stanju, 5 kW donamičkog odziva i -3.6 kVAr reaktivne snage. U eksperimentalnom istraživanju izmjenjivač je upravljan tehnikom prostorno vektorske širinsko-impulsne modulacije u d-q referentnom sustavu te je korištena dSPACE DS1103 upravljačka pločica. Ukupna harmonička distorzija mrežne struje i efikasnost su 3.59% i 97.6%.

Ključne riječi: izmjenjivač spojen na mrežu, modeliranje izmjenjivača, prostorno vektorska širinsko-impulsna modulacija, ukupna harmonička distorzija.

1 INTRODUCTION

Energy transfer from renewable energy sources to the grid is realized with power electronic converters. Depending on the energy source, different power converters can be utilized in distributed power generation systems (DPGSs). DC energy produced by PV panels or fuel cells is generally converted to constant DC voltage with DC/DC converter which provides DC-link of the inverter. In case of wind power systems, the DC-link voltage is obtained with an AC/DC converter. In some applications, an additional DC/DC converter can be used to boost the DC voltage. In the last stage, an inverter converts the DC energy to AC energy in order to transfer the energy from DC-link to the grid [1-5].

In grid connected systems, two basic considerations are THD value of grid current and the power factor of the generated power. The THD value of grid current is required to be less than 5 % [6]. Three-phase currents must be synchronized with related three-phase voltages. In order to satisfy the power quality standards, inverter control and modulation technique have an important role.

Three-phase inverters can be controlled in synchronous rotating frame (d-q), stationary reference frame (α-β) and natural frame (a-b-c). In d-q frame control, three-phase voltages and currents are transformed by Park transformation into the d-q reference frame that rotates synchronously with the grid voltage. Thus, three-phase variables become DC quantities [7]. As the control variables are DC, different filtering methods can be used, and PI controller achieves good performance in this reference frame control. In stationary reference frame, three-phase quantities are transformed into α-β frame by Clarke transformation. Thus the variables become sinusoidal. PI controller cannot regulate the current well, therefore the current has a steady-

state error. PR controller is the most common controller in stationary reference frame. As PR controller is used with α-β quantities, Park transformation can be avoided [8]. The natural reference frame control uses the three-phase grid voltages and currents. Hence, each phase value can be controlled individually. Hysteresis current control (HCC) and linear current control techniques are widely used in stationary reference frame control [9].

In three-phase grid connected inverters, the most commonly used modulation technique is space vector pulse width modulation (SVPWM). This technique controls output voltage vector of inverter and provides optimum switching pattern. Optimum switching decreases the switching frequency and switching losses. The other advantages of SVPWM technique are constant switching frequency, low harmonic content and better DC-link voltage utilization than the conventional sine PWM [10,11].

Grid synchronization has an important role in DPGSs. Different synchronization techniques such as zero crossing, atan function and phase locked loop (PLL) are used in α-β and d-q frame. Zero-crossing technique is the simplest way for grid synchronization. The zero-crossing points of grid voltage are detected every half cycle, and grid frequency is obtained, but this technique has not fast dynamic response to frequency variation [12]. In the atan function technique, the measured grid voltages are transformed into the reference frame, and they are filtered to avoid the effect of notches in the voltage. The delay cancellation techniques are used to increase the performance because filters cause delays in signals. The atan function technique can be realized in d-q or α-β reference frame [13,14]. Another synchronization technique is PLL. It is the most popular and widely used technique, recently. PLL is generally implemented in the d-q reference frame. The q-component of grid voltage is controlled to provide synchronization. It is set to zero, and the error is applied to the PI regulator. The PI regulator output gives grid frequency, and the integration of this frequency generates the grid angle. This angle is used to produce the synchronized reference current [15-17].

In this paper, a 10 kW grid connected three-phase inverter is proposed. The inverter is controlled with SVPWM, and the synchronization is provided with PLL method. The system is modeled in MATLAB, and characteristic curves that show the total harmonic distortion (THD) of grid current for various switching frequencies, DC-link voltages and inductance values are obtained depending on the modeling. The system is simulated in Simulink with selected system parameters from the curves. The simulation and modeling results are verified with experimental results.

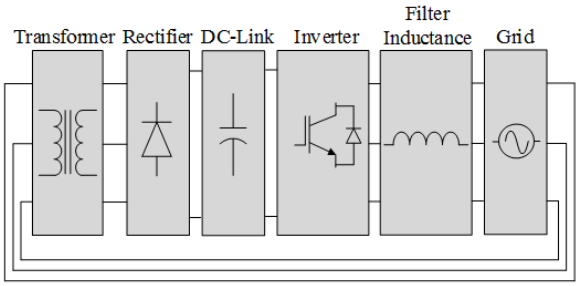

Fig. 1. Block diagram of the grid connected inverter.

2 SYSTEM DESCRIPTION

The block diagram of the three-phase grid connected inverter system is shown in Fig. 1. The DC-link voltage is obtained from three-phase grid with a transformer, a diode rectifier and capacitors. The transformer boosts the voltage and high DC-link voltage is obtained. The three-phase two-level IGBT intelligent power module (IPM) inverter is connected to the grid through L filters. The inverter is controlled with dSPACE 1103 control board.

3 CONTROL ALGORITHM

The control block diagram of the system is shown in Fig. 2. The grid voltages are measured, and grid angle is determined with PLL method. The grid angle is used to transform the grid currents and voltages from a-b-c reference frame to d-q reference frame by Park transformation as given in (1). The error is calculated from the reference and measured d-q currents, and the errors in d-q frame are given to PI regulators. The reference d-component of the current defines the maximum value of the grid current. The q-component current controls the reactive power flow. It is set to zero for only active power injection. PI outputs are summed with feed-forward grid voltage components and decoupling components to produce reference inverter output voltages. The outputs of the PI regulators are transformed into α-β frame using (2). Inverter reference voltages in α-β reference frame and DC-link voltage are used in the SVPWM, and the switching signals are produced.

The reference output voltage vector of inverter (V_{ref}) is shown in Fig. 3. The reference voltage is the sum of α and β components. These values are used for determining sector of the reference voltage vector. It can be achieved with atan function. This function is used to calculate the vector angle.

$$\begin{bmatrix} v_d \\ v_q \end{bmatrix} = \frac{2}{3} \begin{bmatrix} \cos\theta & \cos(\theta - \frac{2\pi}{3}) & \cos(\theta - \frac{4\pi}{3}) \\ -\sin\theta & -\sin(\theta - \frac{2\pi}{3}) & -\sin(\theta - \frac{4\pi}{3}) \end{bmatrix} \begin{bmatrix} v_{ga} \\ v_{gb} \\ v_{gc} \end{bmatrix} \tag{1}$$

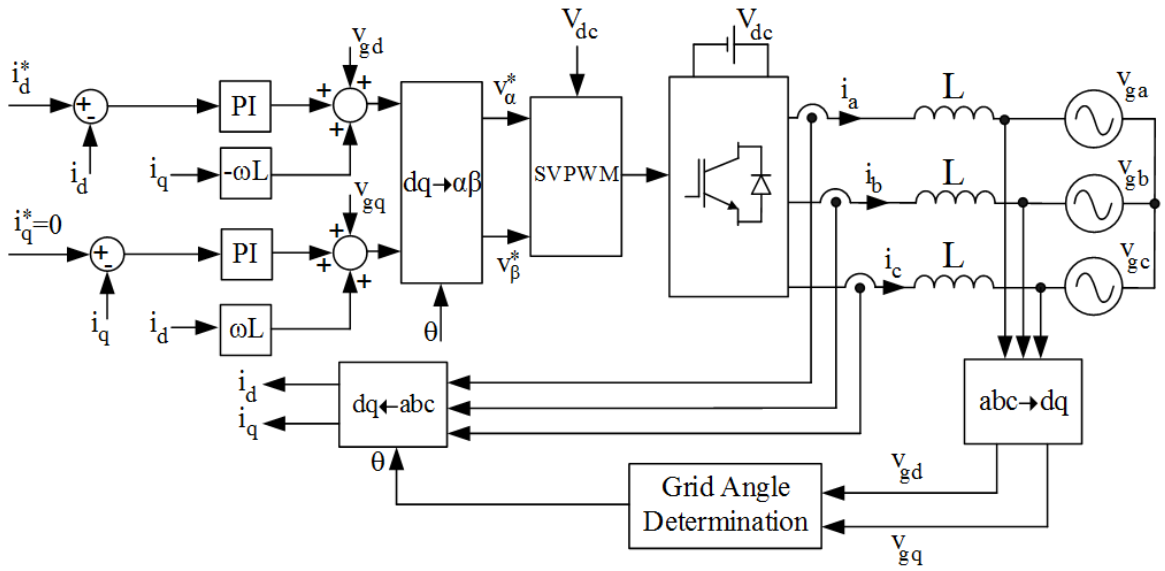

Fig. 2. Control block diagram of the inverter.

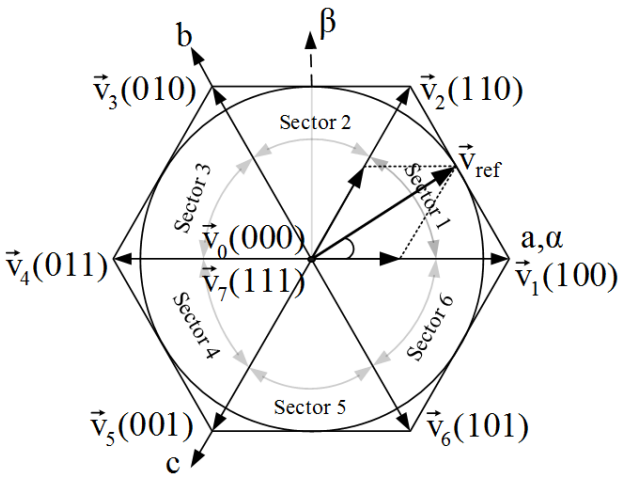

Fig. 3. SVPWM switching sectors.

$$\begin{bmatrix} v_\alpha \\ v_\beta \end{bmatrix} = \begin{bmatrix} \cos\theta & -\sin\theta \\ \sin\theta & \cos\theta \end{bmatrix} \begin{bmatrix} v_d \\ v_q \end{bmatrix} \tag{2}$$

The sector changes in each 60°, therefore the sector of reference vector is determined according to the calculated vector angle. The inverter produces the voltage with combination of two adjacent vectors and zero vectors. There are six active (V_1-V_6) and two zero (V_0,V_7) vectors as shown in Fig. 3. The vector durations are calculated in each sector, and they are applied to the inverter semiconductor switches.

The phase angle of grid voltage is calculated by software PLL. The algorithm block diagram is given in Fig. 4. Grid angle is calculated using the q-component of grid

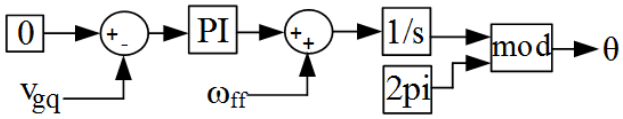

Fig. 4. PLL algorithm block diagram.

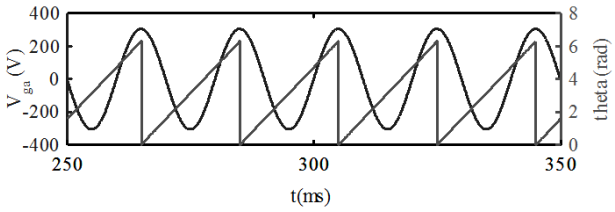

Fig. 5. Grid angle variation.

voltage. The reference value of angle is set to zero. Angle error is given to PI regulator, and it generates angular frequency. The output signal of PI is added to fundamental angular frequency of grid voltage to calculate the actual angular frequency. Instantaneous phase angle is obtained by integrating the angular frequency. Phase angle variation with phase-a grid voltage is seen in Fig. 5.

4 MODELING OF THE SYSTEM

The circuit topology that is modeled for parametric analysis is shown in Fig. 6. It is assumed that three-phase grid voltages are balanced and stable, the switches are ideal, and DC-link voltage is constant.

The system can be modeled in different frames such as d-q, α-β and a-b-c. d-q model of the system is given in (3)

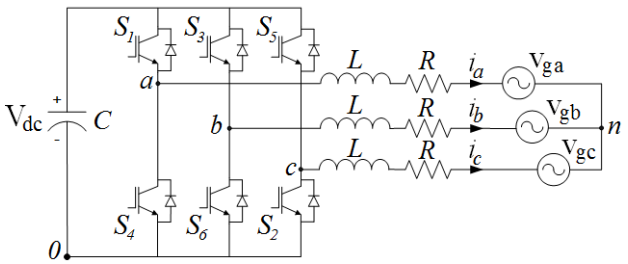

Fig. 6. Three-phase grid connected inverter.

and (4).

$$v_d = L\frac{di_d}{dt} - \omega L i_q + v_{gd} \tag{3}$$

$$v_q = L\frac{di_q}{dt} + \omega L i_d + v_{gq}\,, \tag{4}$$

where v_d and v_q are inverter output voltages, i_d and i_q are grid currents, v_{gd} and v_{gq} are grid voltages, ω is grid frequency and L is inverter output filter inductance.

In this study, the system is modeled in a-b-c reference frame as given in (5)-(7). R is the equivalent series resistance (ESR) value of the inductance. The circuit equation for each phase can be derived as seen in (5). Since the inverter has three-wire, there is a voltage difference (v_{n0}) between neutral point of the grid and negative point of the DC-link. The v_{n0} is defined as a function of inverter output voltages by (6), and the inverter output voltages are defined as a function of leg switching states by (7).

$$v_{k0} = L\frac{di_k}{dt} + Ri_k + v_{gk} + v_{n0} \tag{5}$$

$$v_{n0} = \frac{1}{3}(v_{a0} + v_{b0} + v_{c0}) \tag{6}$$

$$v_{k0} = S_k \cdot V_{dc} = \begin{cases} V_{dc}, & S_k = 1 \\ 0, & S_k = 0 \end{cases} \tag{7}$$

In the equations above, k represents the phase of inverter, $k \in \{a, b, c\}$ and S defines the states of upper switches. When S is 1, the related upper switch is ON and lower switch is OFF in the inverter leg.

Using the (5)-(7), the model of the grid connected inverter can be written in the state-space equation as below.

$$\begin{aligned} \dot{x} &= Ax + Bu \\ y &= Cx \end{aligned} \tag{8}$$

The state and input vectors can be defined by (9) and (10), respectively.

$$x = \begin{bmatrix} i_a & i_b & i_c \end{bmatrix}^T \tag{9}$$

$$u = \begin{bmatrix} v_{a0} - v_{ga} - v_{n0} \\ v_{b0} - v_{gb} - v_{n0} \\ v_{c0} - v_{gc} - v_{n0} \end{bmatrix} \tag{10}$$

The coefficient matrices are given in (11).

$$A = \begin{bmatrix} -\frac{R}{L} & 0 & 0 \\ 0 & -\frac{R}{L} & 0 \\ 0 & 0 & -\frac{R}{L} \end{bmatrix} \quad B = \begin{bmatrix} \frac{1}{L} & 0 & 0 \\ 0 & \frac{1}{L} & 0 \\ 0 & 0 & \frac{1}{L} \end{bmatrix} \tag{11}$$

The output coefficient matrix C is a unity matrix with dimensions of 3×3. The output variables are phase currents of the inverter.

5 MODELING AND SIMULATION RESULTS

The system is modeled and simulated for 10 kW output power in MATLAB and Simulink with m-file and SimPowerSystems Blocksets, respectively. The Simulink block diagram model is shown in Fig. 7.

The system model and control algorithm are run in m-file for parametric analysis. The system is investigated for various parameters, and characteristic curves are obtained as shown in Fig. 8 - Fig. 10. THD variation curves of the grid current with different filter inductance values and switching frequencies for $V_{dc} = 650$ V and 5% THD limit line are shown in Fig. 8.

Increasing the switching frequency and/or inductance value decrease THD value. High value inductance increases voltage drop, volume and cost. For the same THD value with low inductance, switching frequency must be increased, but high switching frequency decreases the inverter efficiency due to the switching losses. The inverter can be switched at lower switching frequencies to increase efficiency, but in this case, the inductance value must be increased as shown in Fig. 8. According to modeling results for 3mH inductance, the THD values of the grid current are 10.22% and 3.41% for 3 kHz and 9 kHz switching frequency, respectively.

Fig. 9 and Fig. 10 show the THD variations of grid current depending on the filter inductance value and DC-link voltage at 3 kHz and 9 kHz switching frequency, respectively. As seen in the figures, high DC-link voltage increases the THD value of grid current because of high voltage drop on filter inductors. Although increasing inductance value provides THD decreasing, 3 kHz kHz switching frequency does not satisfy 5% THD limit for $1 - 5$ mH inductance values. Higher value inductor is needed to meet the THD requirement.

In contrast to low switching frequency (3 kHz), THD value at three times higher switching frequency (9 kHz) meets THD limit with 2 mH and 650 V as shown in Fig. 10.

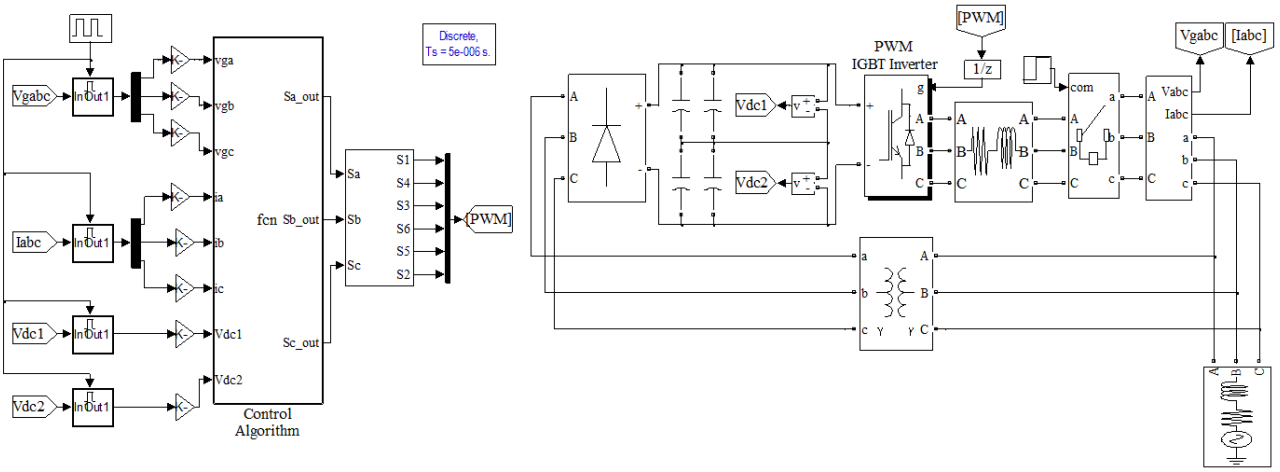

Fig. 7. Control block diagram and power circuit of the system in Simulink.

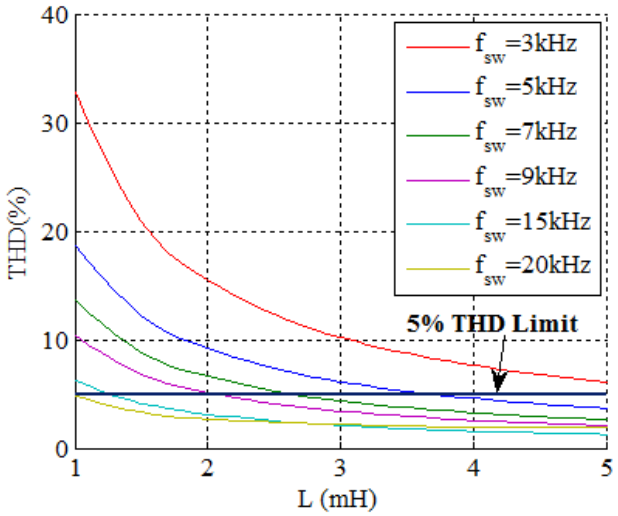

Fig. 8. THD variation of the grid current for $V_{dc} = 650$ V.

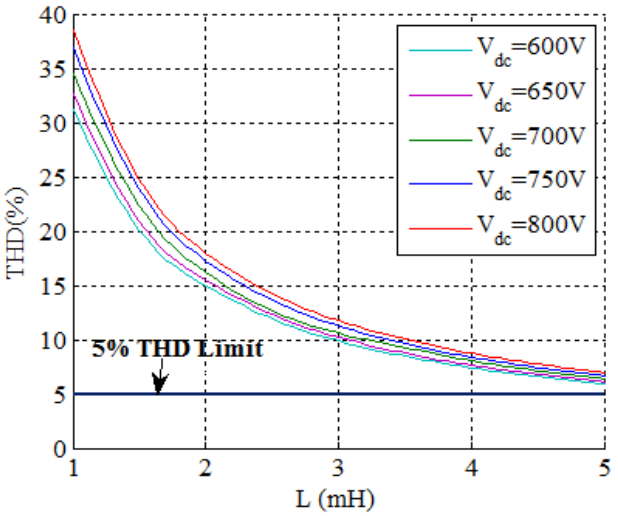

Fig. 9. THD variation of the grid current for $f_{sw} = 3$ kHz.

In simulation study, the DC-link voltage is 650 V, inverter output filter inductance value is 3 mH, ESR value of the inductor is 20 mΩ and grid phase-to-neutral voltage is 220 V. The power circuit is built using SimPowerSystems Blocksets, and control algorithm is implemented with Embedded Matlab Function block. The DC-link is splitted into two capacitors that have 4800 μF capacity. The input phase-to-phase voltage of the transformer is 380 V, and output voltage is 460 V. In the control algorithm, PI controller coefficients of grid regulation are used as $K_P = 3$ and $K_I = 3e - 3$. The waveforms of grid voltages and currents at 3 kHz and 9 kHz can be seen in Fig. 11 – Fig. 14.

The grid currents at 3 kHz switching frequency are given in Fig. 11. The currents are synchronized with grid voltages but the current ripple is high due to low switching frequency. The THD value of the current is 10.22% that does not meet the THD limit. The THD value is the same with the result obtained from the mathematical modeling as shown in Fig. 9. d-q components are shown at 3 kHz switching frequency in Fig. 12, and the current ripple is quite high.

The influence of higher switching frequency on grid current is clearly seen in Fig. 13. In contrast to Fig. 11, grid current ripple is quite less at 9 kHz. The ripple decrement also can be seen from d-q component of grid current in Fig. 14. The current THD value 3.44% is three times less than the THD value at 3 kHz.

Dynamic response of the inverter is considerable in renewable energy conversion systems because of variable

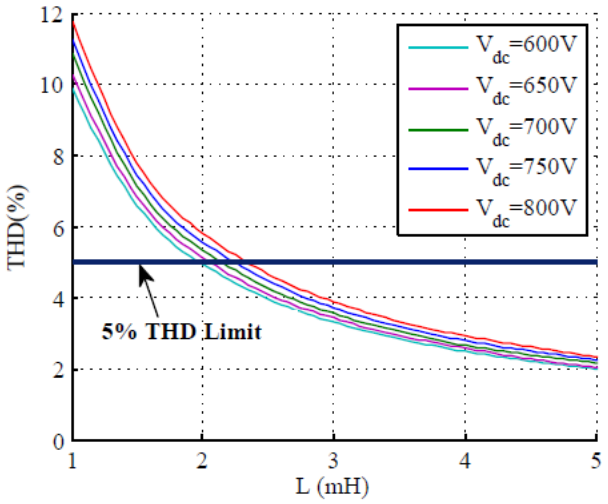

Fig. 10. THD variation of the grid current for f_{sw} = 9 kHz.

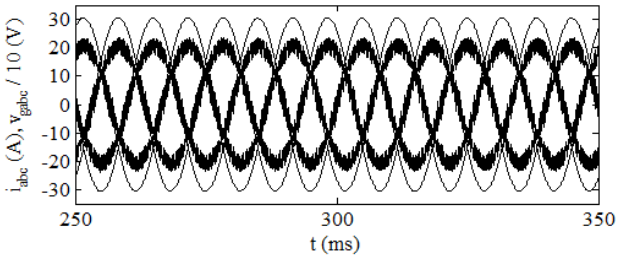

Fig. 11. Three-phase grid currents and voltage for f_{sw} = 3 kHz.

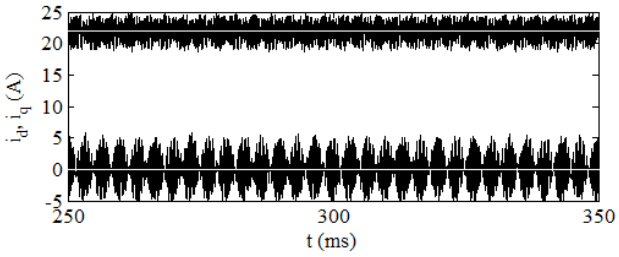

Fig. 12. d-q components of the grid current for f_{sw} = 3 kHz.

wind speed and solar radiation depending on the weather conditions. In the study, PI regulator is used to regulate the grid current in steady state or dynamic response. The dynamic response of the inverter can be seen in Fig. 15-Fig. 17. The reference and actual grid current in dq reference frame are given in Fig. 15. As seen from the figure, id and iq currents are regulated by the controller. d and q components are set to 22 A-11 A-15.5 A and 7.7 A respectively to show the dynamic response and reactive power generation

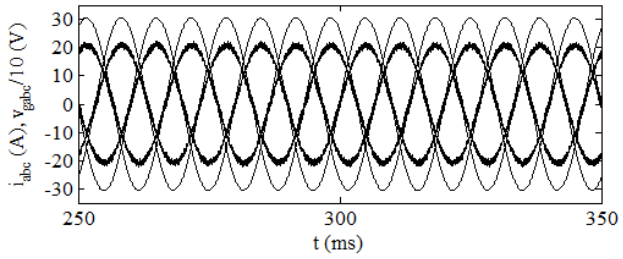

Fig. 13. Three-phase grid currents and voltage for f_{sw} = 9 kHz.

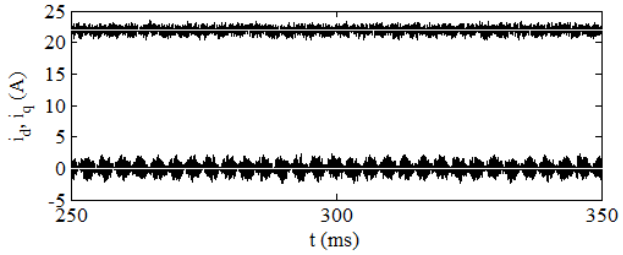

Fig. 14. d-q components of the grid current for f_{sw} = 9 kHz.

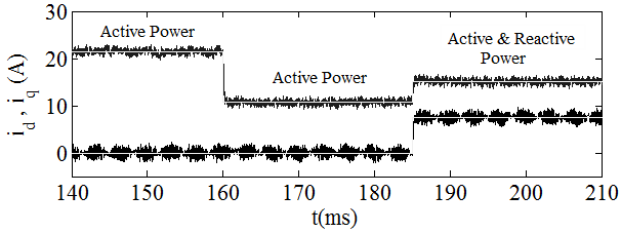

Fig. 15. d-q components of grid current.

capability. Actual currents can track the reference values in dq axis. In Fig. 16, it is clearly seen that during the only active power flow, three-phase grid currents are synchronized with grid voltages. On the contrary, there is a phase shift between currents and voltages in the reactive power flow interval. Output power variation based on the currents and voltages is given in Fig. 17. For three different power level, inverter accomplishes the active and reactive power flow.

6 EXPERIMENTAL STUDY

The experimental block diagram and laboratory prototype for 10 kW power are shown in Fig. 18 and Fig. 19, respectively. The system includes a transformer, a diode rectifier, two DC-link capacitors, a two-level IGBT inverter and filter inductors. The specifications of the inverter prototype are V_{dc} = 650 V, L = 3 mH, f_{grid} = 50 Hz, C_1 and C_2 are 4800 μF, sampling time is 20 μs, f_{sw1} =

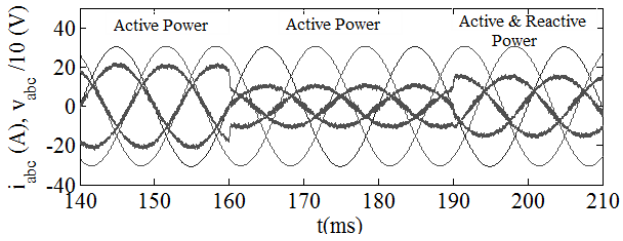

Fig. 16. Three-phase grid currents and voltages.

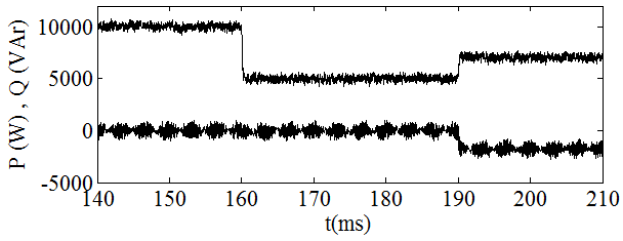

Fig. 17. Output power variation of the inverter.

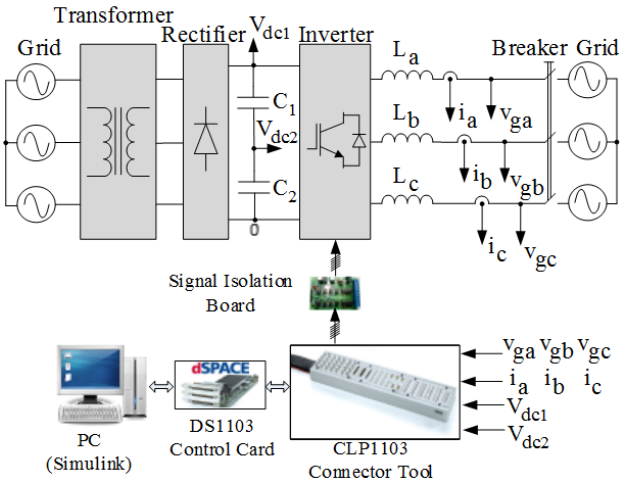

Fig. 18. Experimental setup block diagram.

3 kHz and $f_{sw2} = 9$ kHz. The system control is realized with SVPWM technique. The control algorithm has been implemented using a dSPACE DS1103 board including TMS320F240 DSP. The dSPACE can be programmed with MATLAB/Simulink platform that provides easy programming for DSP.

All currents, voltages in the power circuit and variables in the control algorithm can be monitored using the Controldesk that is a dSPACE software. In addition, parameters such as K_p, K_I and reference signals can be controlled with this program via Real-Time Interface (RTI). The Simulink control model that is developed with SimPowerSystems Blocksets, or software that is written in m-file is converted to C-code with Real-Time Workshop. The

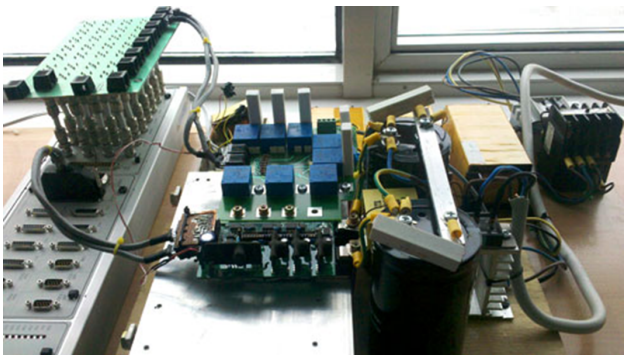

Fig. 19. Laboratory prototype.

dSPACE 1103 has a connector panel (CLP1103) for I/O, ADC, DAC connections.

In the power circuit, Mitsubishi IPM PM50CL1A120 is used as the three-phase two-level inverter. The signal isolation is provided with EVBL1S1XX evaluation board. HCPL4506 and PC817 integrated circuits are used on the board to isolate IGBT gate and module fault signals, respectively. The DC-link voltage is supplied from the grid via a transformer, a three-phase diode rectifier module and DC capacitors. The grid voltage is boosted by the transformer to obtain high DC-link voltage.

Three-phase grid voltages and DC-link voltage are measured with LEM LV25-P sensors. Two voltage sensors are used to measure the DC-link voltage. Each sensor senses half of the DC-link voltage, and total DC-link voltage is calculated in the software. There-phase grid currents are measured with LEM LA25-NP. Five voltages and three currents measurements are given to ADC channels via CLP1103.

In Fig. 20, three-phase grid currents and voltages at 3 kHz switching frequency are given for 10 kW power transfer. The currents are synchronized with related grid voltages but THD value is 10.68%. The current THD value is high and does not meet 5% THD limit because of low switching frequency and inadequate value of L filter. RMS value of the grid current is 14.9 A.

Three-phase grid voltages and currents at 9 kHz switching frequency are given in Fig. 21. The voltage scale (Ch1, ChA, ChB) is 70 V/div, and the current scale (Ch2, ChC, ChD) is 6 A/div. The THD value is 3.59%, and rms value is 15.1 A.

Grid angle that is calculated by PLL and phase-a grid voltage waveforms are seen in Fig. 22. The angle crosses zero points at the peak point moments of phase-a grid voltage as seen from the figure. Thus, coordinate transformations can be done, correctly.

The dynamic response of the inverter is shown in Fig. 23-Fig. 25. Three phase grid currents are given in Fig.

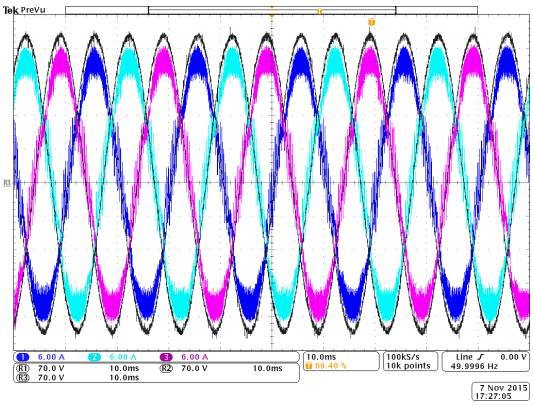

Fig. 20. Three-phase grid currents and voltages for $f_{sw} = 3\,kHz$.

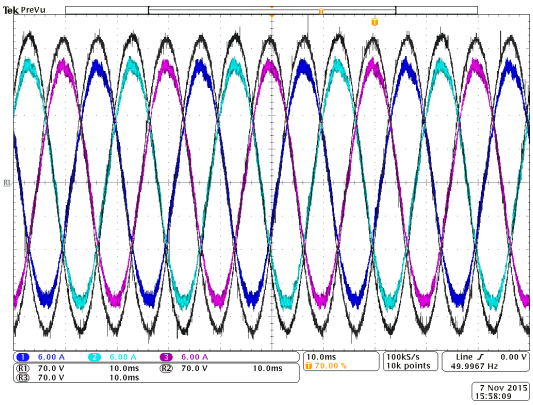

Fig. 21. Three-phase grid currents and voltages for $f_{sw} = 9\,kHz$.

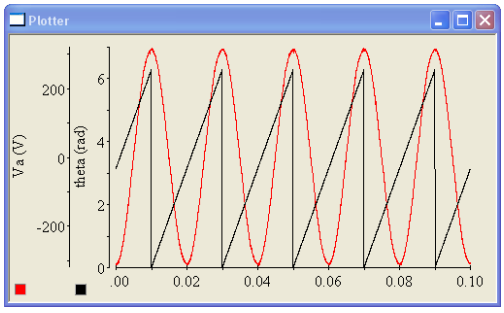

Fig. 22. Phase-a voltage and grid angle.

23. Firstly, the inverter produces 10 kW power, then output power reduces to 5 kW. In the first 70 ms, grid currents are synchronized with grid voltages because of active power producing. As seen from the figure inverter has fast dynamic response to reference change. During the last 30 ms, grid voltages and currents are not synchronized because of reactive power generation. Actual and reference

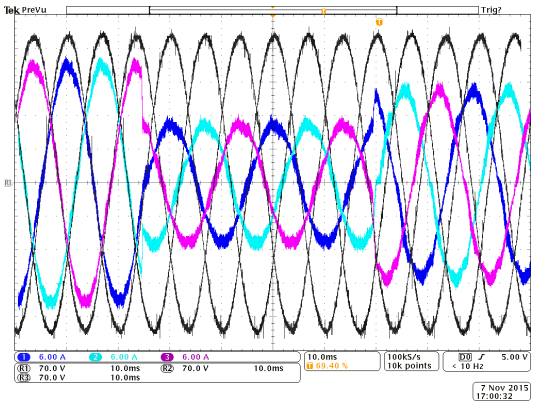

Fig. 23. Dynamic response for $f_{sw} = 9\,kHz$.

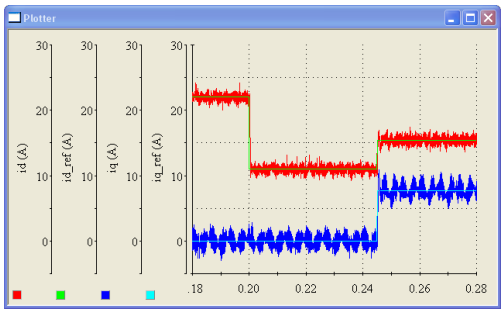

Fig. 24. d-q components of grid current.

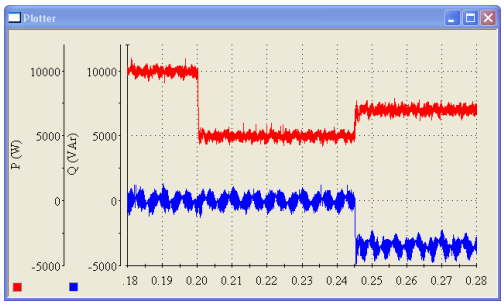

Fig. 25. Active & reactive power.

dq-components of grid currents are given in Fig. 24. q-component is set to zero for no reactive power whereas d-component controls the active power. q-component is generated for reactive power.

Fig. 25 shows the output power variation in ControlDesk plotter that is a software of dSPACE hardware. It has three power level 10 kW, 5 kW and 7.2 kW-3.6 kVAr. Active and reactive power generation capability of the inverter can be seen from the figure clearly.

The obtained grid current THD values from modeling, simulation and experimental studies are given in Table 1. As seen in the table, modeling and simulation results are

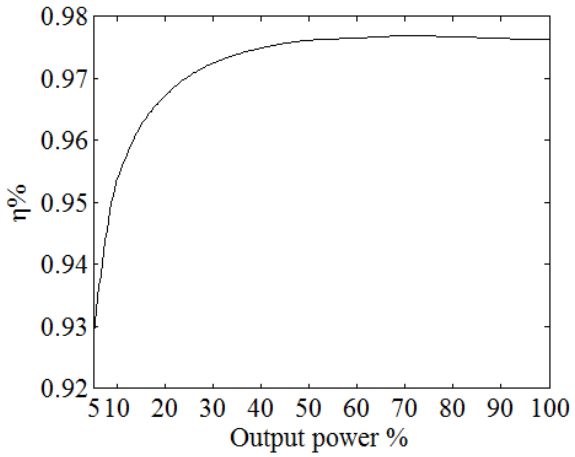

Fig. 26. Efficiency curve of the inverter.

verified with experimental results. The control algorithm used in modeling is run via Embedded Matlab Function in simulation and experimental study. As the same code in Embedded Matlab Function is used in dSPACE control board, very close results are obtained in simulation and experimental study.

Table 1. Grid current THD values for different methods

	Modeling	**Simulation**	**Experimental**
3 kHz	10.22%	10.22%	10.68%
9 kHz	3.41%	3.44%	3.59%

The efficiency curve of the inverter at 9 kHz is given in Fig. 26. Full power efficiency is 97.6% and European efficiency is 97.2%.

7 CONCLUSION

In this study, performance of a 10 kW three-phase grid connected inverter is investigated for various filter inductance values, DC-link voltages and switching frequencies. The system is modeled in m-file, thus characteristic curves of the inverter are obtained for different parameters. The THD values of grid current for 3 kHz and 9 kHz with 650 V DC-link voltage are 10.22% and 3.41%. For verification of the modeling results, the system is simulated in Simulink. The control algorithm is implemented in Embedded Matlab Function in the simulation. The results are compared at 3 kHz and 9 kHz switching frequency, and modeling results are verified with simulation results that are 10.22% are 3.44%. In order to verify the modeling and simulation results, a laboratory prototype that is controlled by dSPACE DS1103 control board is realized. In the experimental study, THD values are measured as 10.68% and 3.59%. Furthermore, dynamic response and reactive power generation capability of the inverter are presented. The experimental results verify the modeling and simulation results. This verification shows that the system can be designed for various system and control parameters using the design curves. The study is realized for 10 kW power but it is possible to obtain the characteristic curves for different power values. According to results, the switching frequency or filter inductance value should be high to meet THD limit. Furthermore, efficiency is another important performance indicator. The efficiency at rated power and the european efficiency of the inverter is 97.6% and 97.2% at 9 kHz.

ACKNOWLEDGEMENTS

This work was supported by The Scientific and Technological Research Council of Turkey (TUBITAK) under grant 110E212.

[1] F. Blaabjerg, M. Liserre and K. Ma: "Power Electronics Converters for Wind Turbine Systems", *IEEE Transaction on Industry Applications*, vol.48, pp. 708-719, 2012.

[2] F. Blaabjerg, Z. Chen, S.B. and Kjaer: "Power Electronics as Efficient Interface in Dispersed Power Generation Systems", *IEEE Transactions on Power Electronics*, vol. 19, pp. 1184-1194, 2004.

[3] J.M. Carrasco, L.G. Franquelo, J.T. Bialasiewicz, E. Galvan, R.C.P. Guisado, M.A.M. Prats, J.I. Leon and N.M. Alfonso: "Power-Electronic Systems for the Grid Integration of Renewable Energy Sources: A Survey", *IEEE Transactions on Industrial Electronics*, vol. 53, pp. 1002-1016, 2006.

[4] C. Ramonas and V. Adomavicius: "Research of the Converter Possibilities in the Grid-tied Renewable Energy Power Plant", *Elektronika IR Elektrotechnika*, vol. 19, pp. 37-40, 2013.

[5] D. Meneses, F. Blaabjerg, O. Garcia and J.A. Cobos: "Review and Comparison of Step-Up Transformerless Topologies for Photovoltaic AC-Module Application", *IEEE Transactions on Power Electronics*, vol. 28, pp. 2649-2663, 2013.

[6] Characteristic of the Utility Interface for Photovoltaic (PV) Systems, *IEC Standard 1727*, 2002.

[7] M. Singh, V. Khadkikar and A. Chandra: "Grid synchronisation with harmonics and reactive power compensation capability of a permanent magnet synchronous generator-based variable speed wind energy conversion system", *IET Power Electronics*, vol. 4, pp. 122-130, 2011.

[8] A. Vidal, F.D. Freijedo, A.G. Yepes, P.F. Comesana, J. Malvar, O. Lopes and J.D. Gandoy: "Assessment and Optimization of the Transient Response of Proportional-Resonant Current Controller for Distributed Power Generation Systems", *IEEE Transactions on Industrial Electronics*, vol .60, pp. 1367-1383, 2013.

[9] E. Isen and A.F. Bakan: "Comparison of Hysteresis Controlled Three-Wire and Split-Link Four-Wire Grid Connected Inverters", *in Proc. 8th Int. Conf. on Electrical Engineering/Electronics, Computer, Telecommunications and Information Technology*, Khon Kaen, Thailand, pp. 727-730, 2011.

[10] L. Yan, X. Li, H. Hu and B. Zhang: "Research on SVPWM Inverter Technology in Wind Power Generation System", *in Proc. International Conference on Electrical and Control Engineering*, Yichang, China, pp. 1220-1223, 2011.

[11] E. Adzic, Z. Ivanovic, M. Adzic and V. Katic: "Maximum Power Search in Wind Turbine Based on Fuzzy Logic Control", *Acta Polytechnica Hungarica*, vol. 6, pp. 131-149, 2009.

[12] F.M. Gardner, Phase Lock Techniques. New York, NY, *USA: Wiley*, 1979.

[13] C. Klumpner, M. Liserre and F. Blaabjerg: "Improved Control of an Active-Front-End Adjustable Speed Drive with a Small DC-link Capacitor under Real Grid Conditions", *in Proc. IEEE 35th Annual Power Electronics Specialists Conference*, Aachen, Germany, pp. 1156-1162, 2004.

[14] X. Qiu, J. Xiao, C. Wu: "Research of Variable Gain Nonlinear PI Controller based Three-Phase Phase-Locked-Loop System", *in Proc. International Conference on Electrical and Control Engineering*, Wuhan, China, pp. 4050-4053, 2010.

[15] S.K. Chung: "A Phase Tracking System for Three Phase Utility Interface Inverters", *IEEE Transactions on Power Electronics*, vol. 15, pp. 431-438, 2000.

[16] X.Q. Guo and W.Y. Wu: "Simple synchronisation technique for three-phase grid-connected distributed generation systems", *IET Renewable Power Generation*, vol. 7, pp. 55-62, 2013.

[17] M. Pastor and J. Dudrik, "Predictive Current Control of Grid-tied Cascade H-bridge Inverter", *Automatika Journal of Control, Measurement, Electronics, Computing and Communications*, vol. 54, no. 3, 308-315, 2013.

Evren Isen was born in Bandirma, Turkey, in 1981. He received B.S. degree in electrical engineering, M.S. degree in electrical engineering, and Ph.D. degree in electrical engineering from Yildiz Technical University, Yildiz, Turkey, in 2003, 2005, and 2012, respectively. Since 2012, he has been working as an Assistant Professor in the Department of Electrical and Electronics Engineering, Kirklareli University. His research interests include grid-connected inverters, wind energy and photovoltaic energy conversion systems in power electronics.

Ahmet Faruk Bakan was born in Istanbul, Turkey, in 1972. He received B.S. degree in electronics and communication engineering, M.S. degree in electrical engineering, and Ph.D. degree in electrical engineering from Yildiz Technical University, Yildiz, Turkey, in 1994, 1997, and 2002, respectively. Since 2012, he has been working as an Associate Professor in the Department of Electrical Engineering, Yildiz Technical University. He has published more than 20 journal and conference papers in the area of power electronics. He was also employed in several research projects concerning power electronics. His research interests include direct torque control, photovoltaic inverters, welding machines, and soft-switching techniques in power electronics.

AUTHORS' ADDRESSES

Evren Isen, Ph.D.,
Kirklareli University,
Department of Electrical & Electronics Engineering,
39000, Kirklareli, Turkey.
email: evren.isen@klu.edu.tr

A. Faruk Bakan, Ph.D.,
Yildiz Technical University,
Department of Engineering & Electronics Engineering,
34220, Istanbul, Turkey.
email: fbakan@yildiz.edu.tr

Received: 2014-10-26
Accepted: 2016-03-02